



HAL
open science

Development of MWCNTs@PDMS nanocomposites with enhanced hydrophobicity and thermo-oxidative stability

Iryna Sulym, Olena Goncharuk, Liudmyla Storozhuk, Konrad Terpilowski, Dariusz Sternik, Eugen Pakhlov, Sombel Diahham, Zarel Valdez Nava

► To cite this version:

Iryna Sulym, Olena Goncharuk, Liudmyla Storozhuk, Konrad Terpilowski, Dariusz Sternik, et al.. Development of MWCNTs@PDMS nanocomposites with enhanced hydrophobicity and thermo-oxidative stability. *Applied Surface Science*, 2024, 667, pp.160405. 10.1016/j.apsusc.2024.160405. hal-04658954

HAL Id: hal-04658954

<https://hal.science/hal-04658954>

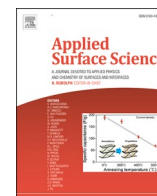
Submitted on 22 Jul 2024

HAL is a multi-disciplinary open access archive for the deposit and dissemination of scientific research documents, whether they are published or not. The documents may come from teaching and research institutions in France or abroad, or from public or private research centers.

L'archive ouverte pluridisciplinaire **HAL**, est destinée au dépôt et à la diffusion de documents scientifiques de niveau recherche, publiés ou non, émanant des établissements d'enseignement et de recherche français ou étrangers, des laboratoires publics ou privés.



Distributed under a Creative Commons Attribution - NonCommercial - ShareAlike 4.0 International License



Full Length Article

Development of MWCNTs@PDMS nanocomposites with enhanced hydrophobicity and thermo-oxidative stability

Iryna Sulym^{a,b,*}, Olena Goncharuk^c, Liudmyla Storozhuk^d, Konrad Terpilowski^e, Dariusz Sternik^e, Eugen Pakhlov^b, Sombel Diahm^a, Zarel Valdez-Nava^a^a LAPLACE, Université de Toulouse, CNRS, INPT, UPS, Toulouse, France^b Chuiko Institute of Surface Chemistry of NAS of Ukraine, 17 General Naumov str., 03164 Kyiv, Ukraine^c Institute of Agrophysics, PAS, Doświadczalna 4, 20-290 Lublin, Poland^d UCL Healthcare Biomagnetics Laboratories, University College London, 21 Albemarle Street, London W1S 4BS, UK^e Maria Curie-Skłodowska University, M. Curie-Skłodowska sq. 3, 20031 Lublin, Poland

ARTICLE INFO

Keywords:

MWCNTs@PDMS nanocomposites
Hydrophobicity
TEM
Raman spectroscopy
Thermo-oxidative stability
Electrical properties

ABSTRACT

This paper presents the fabrication of hydrophobic polymer nanomaterials with improved thermal characteristics based on MWCNTs and poly(dimethylsiloxane). The samples were synthesized by physical adsorption of poly(dimethylsiloxane) onto P-MWCNTs surfaces in the amount from 5 to 20 wt%. The effect of different content of adsorbed polymer on the structure and properties of the prepared nanocomposites was studied in detail using ATR-FTIR, SEM, TEM, XRD and RS techniques. XPS results showed that with the increase of adsorbed PDMS onto the MWCNTs surfaces, the Si 2p atomic percentage increased from 1.5 to 5.0 at. %. The investigation of thermal properties using TGA/DSC techniques in air atmosphere revealed that polymer adsorption on the MWCNTs surfaces enhances the thermo-oxidative stability of the nanocomposites to a great extent. The WCA of MWCNTs@PDMS-1000(20) nanocomposite reached 138.9° while this value was 81.8° in the case of the P-MWCNTs. The electrical characterization of the examined samples demonstrated a non-linear current-voltage behaviour and the invariance of the electrical current value with the increasing polymer content in the nanocomposites. The results suggest that the obtained nanocomposites have multi-functional surfaces and are promising for integration into a silicon-based polymer matrix for the development of new materials for electronic devices.

1. Introduction

In recent decades, hydrophobic/superhydrophobic surfaces has been intensively investigated and remarkable progress has been made [1–4]. Obtaining innovative, non-toxic and multi-functional materials with a high degree of hydrophobicity production is an important task for the academic and industrial environments. Hydrophobic/superhydrophobic materials have potential multi-use applications, namely: self-cleaning hydrophobic coatings, chemical separation of polar and non-polar substances, supports for enzymes, adsorption of organic contaminants, oil/water separation, drag-reducing gas, as thickeners and fillers for non-polar media [5–8]. Surface wettability is one of the important and crucial characteristics for determining of the material use in specific application [9]. Estimation of wettability is based on the measurement of the material surface contact angle (CA). For contact angles less than

90°, the surface is described as hydrophilic, if the contact angle varies between 90° and 150°, the surface is hydrophobic, and if the water contact angle is greater than 150° with a sliding angle (SA) of less than 10°, the surface is considered as superhydrophobic [4,10]. It was established that the wettability of a solid surface is governed by both the surface chemical composition and the surface geometrical microstructures [2]. Changes in these parameters can adjust the value of the contact angle and, therefore, wettability. As for multi-functional surfaces, one can think of the hydrophobic/superhydrophobic surface with such additional properties as magnetic, thermal and electrical conductivities. These functionalities can be achieved using hydrophobic polymers and various nanofillers, in particular, carbon-based materials such as carbon nanotubes, graphite, graphene oxide, activated carbons, fullerenes, micro-/meso-porous carbon etc. [11–15]. Recently, superhydrophobic surfaces based on multi-walled carbon nanotubes (MWCNTs) have been

* Corresponding author at: LAPLACE, Université de Toulouse, CNRS, INPT, UPS, Toulouse, France

E-mail address: iryna.sulym@laplace.univ-tlse.fr (I. Sulym).<https://doi.org/10.1016/j.apsusc.2024.160405>

Received 11 December 2023; Received in revised form 27 May 2024; Accepted 27 May 2024

Available online 28 May 2024

0169-4332/© 2024 The Authors. Published by Elsevier B.V. This is an open access article under the CC BY license (<http://creativecommons.org/licenses/by/4.0/>).

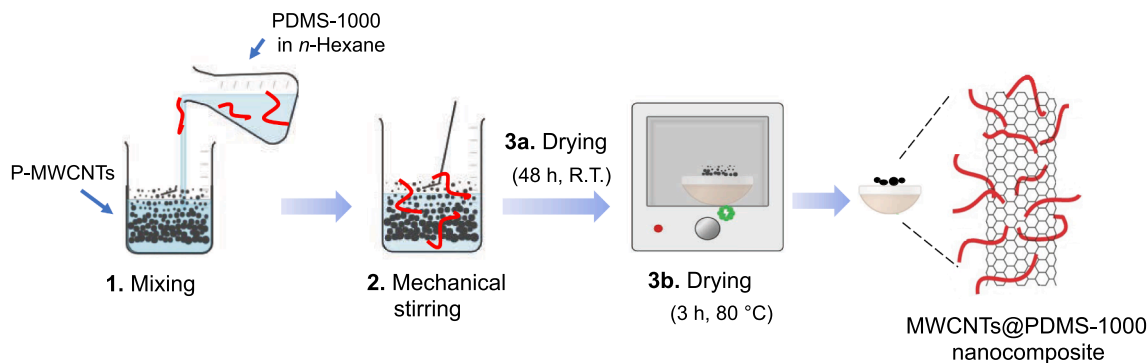


Fig. 1. Schematic view of the main stages of polymer nanocomposites preparation based on MWCNTs and PDMS-1000.

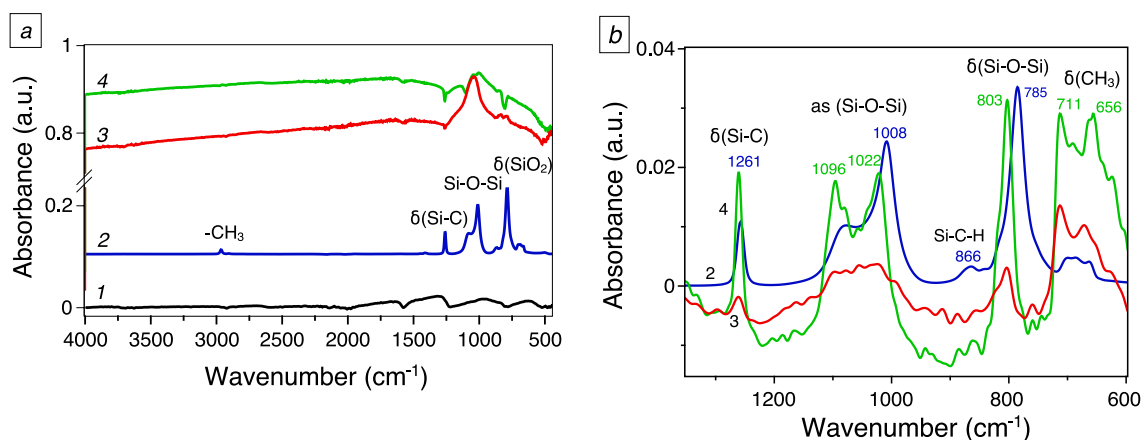


Fig. 2. FTIR spectra of P-MWCNTs (1), neat PDMS-1000 (2), MWCNTs@PDMS-1000(5) (3) and MWCNTs@PDMS-1000(20) (4) nanocomposites: (a) ATR and (b) with dilution in paraffin oil.

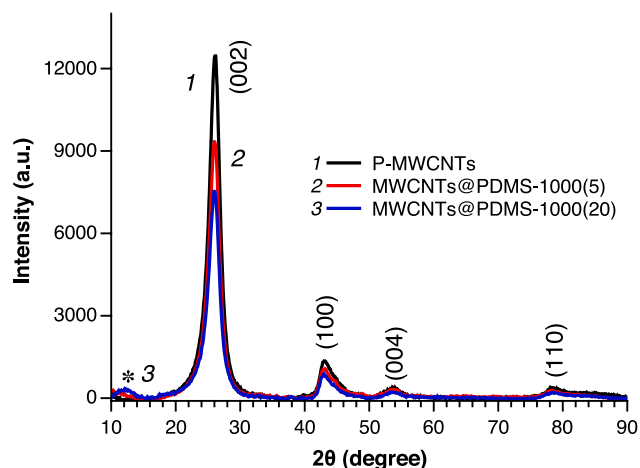


Fig. 3. XRD patterns of P-MWCNTs (1), MWCNTs@PDMS-1000(5) (2) and MWCNTs@PDMS-1000(20) (3) nanocomposites. (*) Lines corresponding to PDMS tetragonal phase.

fabricated because of their promising applications such as conductive-transparent films, oil-water separation, sensors, robust and lightweight composites, electrochemical and electronic devices, as well as electromagnetic interference shielding [16–20]. The MWCNTs include several to tens of incommensurate concentric cylinders of graphitic shells with a layer spacing of 0.3–0.4 nm and tend to have diameters in the range 2–100 nm. They exhibit large specific surface area, porosity, hollow structure, mechanical flexibility, electrical conductivity, thermal

and chemical stability, excellent chemical tunability [11,14,18]. Furthermore, MWCNTs are able to create a surface in both microscale and nanoscale, owing to their rigid cylindrical nanostructure. Based on this, multi-walled carbon nanotubes were used as a substrate. In most studies, poly(dimethylsiloxane) (PDMS) is commonly used as a low surface energy polymer (~ 19.6 mJ/m²) [21] to develop hydrophobic/superhydrophobic surface due to its versatility, which includes a high degree of water-repelling, low cost, nontoxicity, high flexibility, chemical inertness, electrical insulation capability [22] and thermal stability over a large temperature range [10,23]. To this end, in this research, PDMS was considered as an effective modifier for the surface adsorption of hydrophilic MWCNTs. The chemical structure of PDMS consists of inorganic (Si-O) backbone and repeating (Si(CH₃)₂O)_n Si(CH₃)₃, where *n* is the number of units, that are repeated [24]. In addition, (CH₃) represents the methyl group and (Si-O) corresponds to the strength of the siloxane bonds that make this material chemically and thermally stable. According to the literature [25], the PDMS-CNTs interfacial interaction is preferential due to the interaction between the methyl groups of the polymer and the π -electron-rich surface of the carbon nanotubes (so called *CH- π* interaction), in addition to the ability of PDMS to wrap the CNTs. Following the technological developments, the understanding of CNTs-polymer interaction is mandatory for the creation of a new generation of CNTs-polymer nanocomposites with targeted end properties. In this context, the investigation of the thermal behavior of polymer nanocomposites are extremely important for understanding the stability and performance of components and devices composed of these materials [26,27]. Nevertheless, there are no comprehensive studies on the physical modification of surface MWCNTs with linear hydrophobic PDMS and further characterization of the structure of such polymer

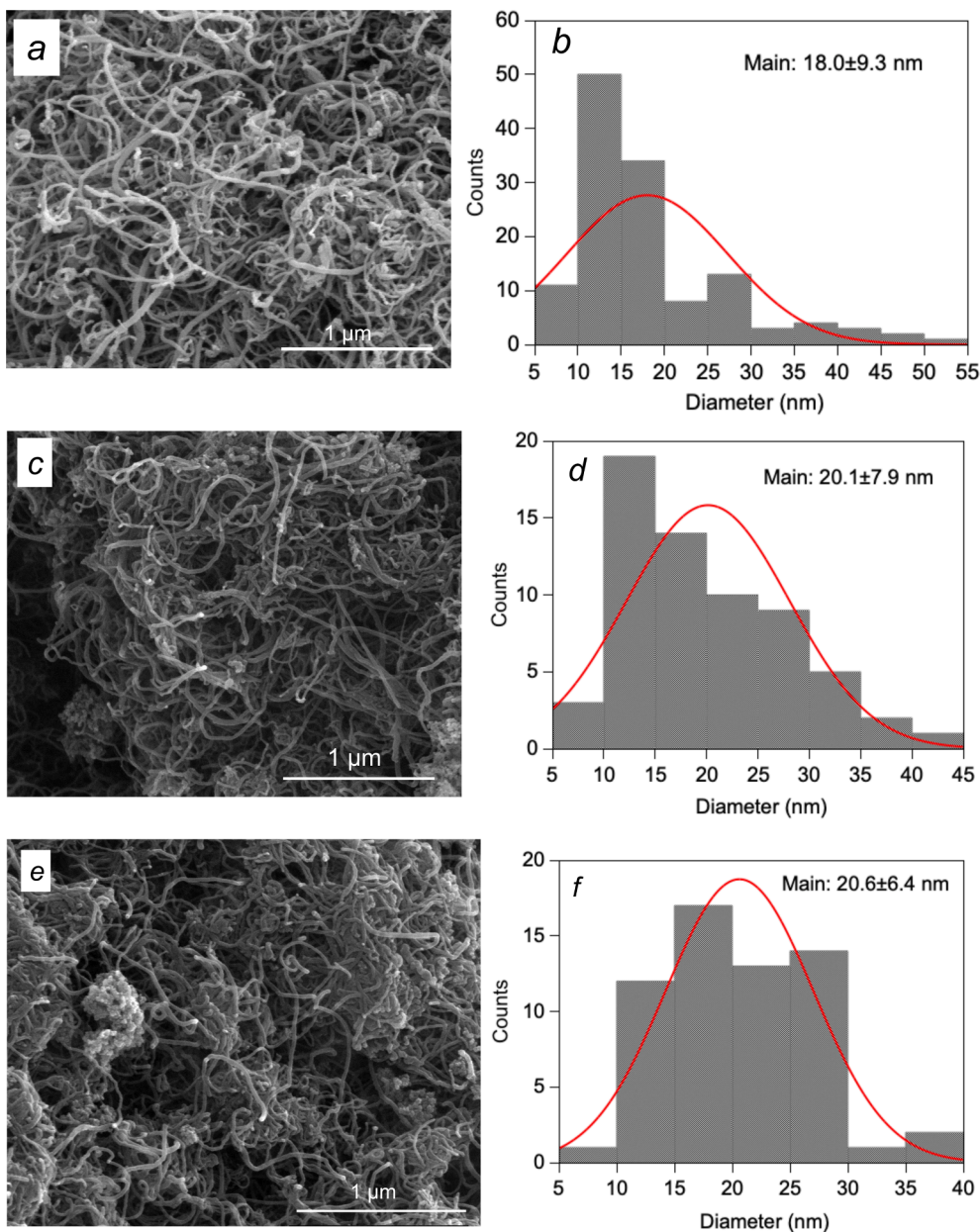


Fig. 4. SEM images (left) used for diameter (right) distributions of the P-MWCNTs (a), MWCNTs@PDMS-1000(5) (c) and MWCNTs@PDMS-1000(20) (e) nanocomposites.

composites in the available literature. In addition, non-covalent modification of carbon nanotubes with poly(dimethylsiloxane) is of particular interest because it does not impair their physical and electrical properties.

For this purpose, this experimental paper focused on the designing of hydrophobic MWCNTs@PDMS nanocomposites and detailed investigation of their structural/textural, thermal and electrical features. The influence of different amounts of physically adsorbed polymer and the structure of MWCNTs on the hydrophobic performance of the prepared nanocomposites was analyzed by the water contact angle and sliding angle measurements. This study is continuation of our previous works concerning the effect of the carbon-based materials on the physico-chemical properties of resulting polymer nanocomposites and their use them as supports for lipase immobilization as well as electrochemical sensor [28–30].

2. Experimental

2.1. Materials

Multi-walled carbon nanotubes (MWCNTs, the average diameter 10–20 nm) were prepared by the catalytic chemical vapour deposition method (CCVD) [31] using pyrolysis of propylene on complex metal oxide catalysts [32]. Then they were used as nanosubstrates. Commercial fluid poly(dimethylsiloxane) PDMS-1000 (Wacker Chemie AG, Munich, Germany, linear, $-\text{CH}_3$ terminated; molecular weight $MW \approx 7960$ g/mol and degree of polymerization $d_p = 105$) served as a hydrophobic polymer for the MWCNTs@PDMS nanocomposite system. *n*-Hexane (≥ 97.0 % GC, Sigma-Aldrich, Germany) was chosen as the solvent. The paraffin oil (Biomus, Lublin, Poland) was used for the FTIR measurements. The conducting silver paste (EPO-TEK® H20E, Orgeval, France) is a thermosetting epoxy loaded with silver particles being used for electrical contact with the nanocomposites, and supplied by Epoxy

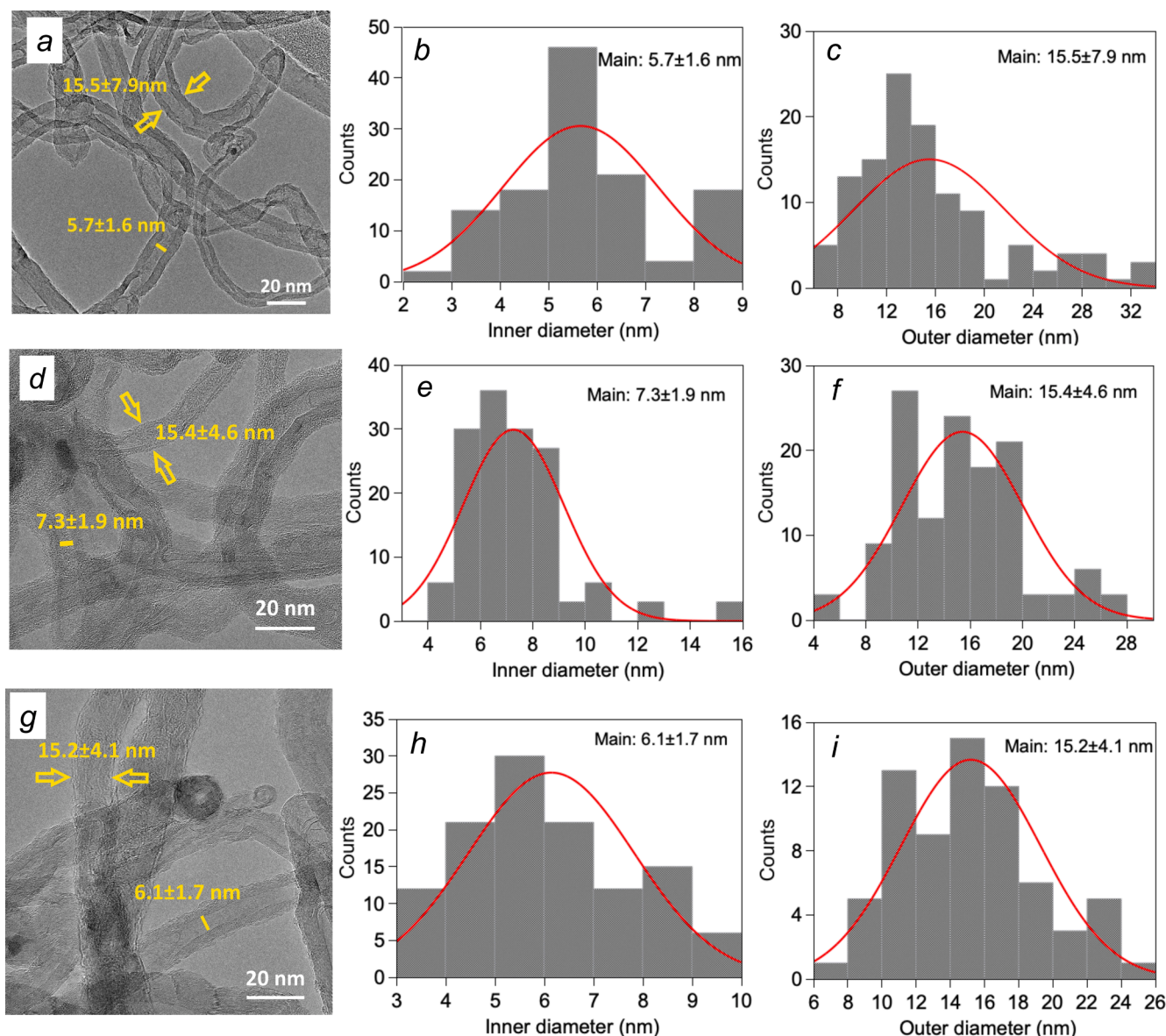


Fig. 5. TEM images (left) used for measurement of inner diameter (center), and outer diameter (right) distributions of the P-MWCNTs (a), MWCNTs@PDMS-1000(5) (d), and MWCNTs@PDMS-1000(20) (g) nanocomposites.

Technology Europe SAS. It is available in two parts; both part A and part B have silver particles dispersed in them. They are mixed in a ratio of 2:1.

2.2. Preparation of MWCNTs@PDMS-1000 nanocomposites

A series of samples was synthesized by the method of physical adsorption of PDMS-1000 onto pristine multi-walled carbon nanotubes (P-MWCNTs) in the amount of 5, 10, 15 and 20 wt% (Fig. 1). Based on our previous report [33], the following procedure was implemented, described as follows: 1) before the modification, P-MWCNTs were dried at 110 °C for 2 h; 2) then a hexane solution of PDMS-1000 (1 wt% PDMS-1000) was prepared and the calculated amount of the solution was added to a fixed mass of dried carbon nanotubes; 3) after that, the suspensions were mechanically stirred for obtaining homogeneity and dried at room temperature for 48 h and then at 80 °C for 3 h to form a powder (similar to P-MWCNTs). The prepared polymer nanocomposites were labelled as MWCNTs@PDMS-1000(5), MWCNTs@PDMS-1000(10), MWCNTs@PDMS-1000(15) and MWCNTs@PDMS-1000(20).

2.3. Characterization of MWCNT@PDMS-1000 nanocomposites

Fourier-transform infrared spectroscopy (FTIR) was done by a ThermoNicolet iS10 FTIR spectrometer. FTIR spectra of powdered samples over the 4000–400 cm^{-1} range with a 4 cm^{-1} spectral resolution by averaging 64 scans were recorded in the ATR mode and with diluted composite samples in paraffin oil. The spectrum of paraffin oil was taken from the ones of composite samples. All spectra presented as absorbance spectra were smoothed and baseline aligned.

X-ray powder diffractograms (XRD) of P-MWCNTs and polymer nanocomposites were obtained on a universal Empyrean diffractometer (Malvern Panalytical) using Cu $K\alpha$ radiation ($\lambda = 0.154 \text{ nm}$) over the 2 θ range of 10–90°.

The morphological investigations were carried out by transmission electron microscopy (TEM) and scanning electron microscopy (SEM). The SEM images were recorded using a QuantaTM 3D FEG (FEI Company, USA) apparatus operating at a voltage of 30 kV. Powdered samples were placed on the circular aluminum stubs with double sticky carbon tape and then covered with Pd/Au (EM SCD005, Leica). TEM images were captured using a Tecnai G2 T20 X-TWIN (FEI Company, USA)

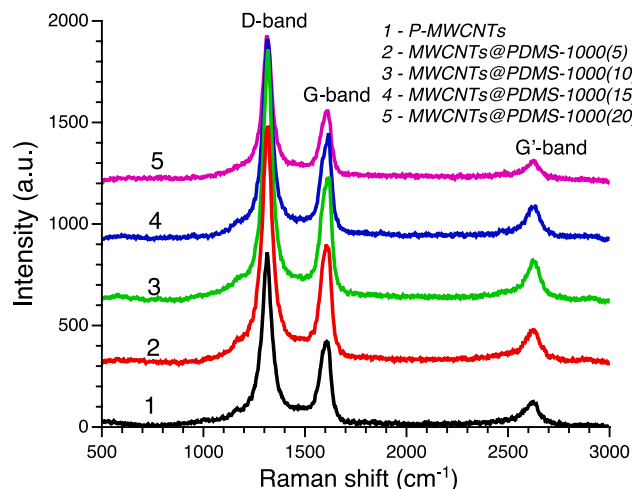


Fig. 6. Raman spectra of P-MWCNTs (1) and MWCNTs@PDMS-1000 (2–5) nanocomposites.

Table 1

XPS analysis results of P-MWCNTs and MWCNTs@PDMS-1000 nanocomposites.

Sample	Element	Peak position (eV)	At. conc. %	Total %
P-MWCNTs	C 1s	284.0	95.3	100.0
	O 1s	533.0	4.7	
MWCNTs@PDMS-1000 (5)	C 1s	284.5	95.8	100.0
	O 1s	532.0	2.7	
	Si 2p	101.5	1.5	
MWCNTs@PDMS-1000 (15)	C 1s	284.5	90.0	100.0
	O 1s	532.0	5.0	
	Si 2p	101.5	5.0	

apparatus operating at a voltage of 200 kV with electron source. Samples were prepared by pipetting 5 μL of the sample onto carbon-coated copper TEM grids, which were allowed to dry at room temperature. An open-source image processing software ImageJ 1.53a, Java 1.8.0_112 [64-bit] was used to analyze the size distributions from TEM and SEM images. The size (inner and outer diameters of MWCNTs before and after polymer modification) distributions were generated by measuring a minimum of 200 particle's diameters in the TEM and SEM images, respectively.

The Raman spectra were recorded over the 3000–500 cm^{-1} range using an inVia Reflex Microscope DMLM Leica Research Grade, Reflex (Renishaw, UK) with the laser excitation at $\lambda_0 = 514 \text{ nm}$. Each sample was measured at several points with 1 cm^{-1} resolution, and the average results were plotted in this paper.

X-ray photoelectron spectroscopy (XPS) investigations of P-MWCNTs and polymer nanocomposites were conducted using a multi-chamber UHV system (PREVAC, Rogów, Poland). A hemispherical Scienta R4000 electron analyser was utilized to acquire the spectra. To complement the equipment, a Scienta SAX-100 x-ray source (Al $K\alpha$, 1486.6 eV, 0.8 eV band) along with the XM 650 X-Ray Monochromator (0.2 eV band) were used. The analyser's pass energy was set to 200 eV for survey spectra (with 750 meV steps) and 50 eV for regions (high-resolution spectra): C 1s, O 1s, and Si 2p with a 50 meV step. The analysis chamber's base pressure was $2 \cdot 10^{-9}$ mbar, which did not exceed $6 \cdot 10^{-9}$ mbar during the spectra collection. All spectra in the section and analysis have been performed using the same equipment and under identical conditions. The data fitting process has been carried out using the CasaXPS software.

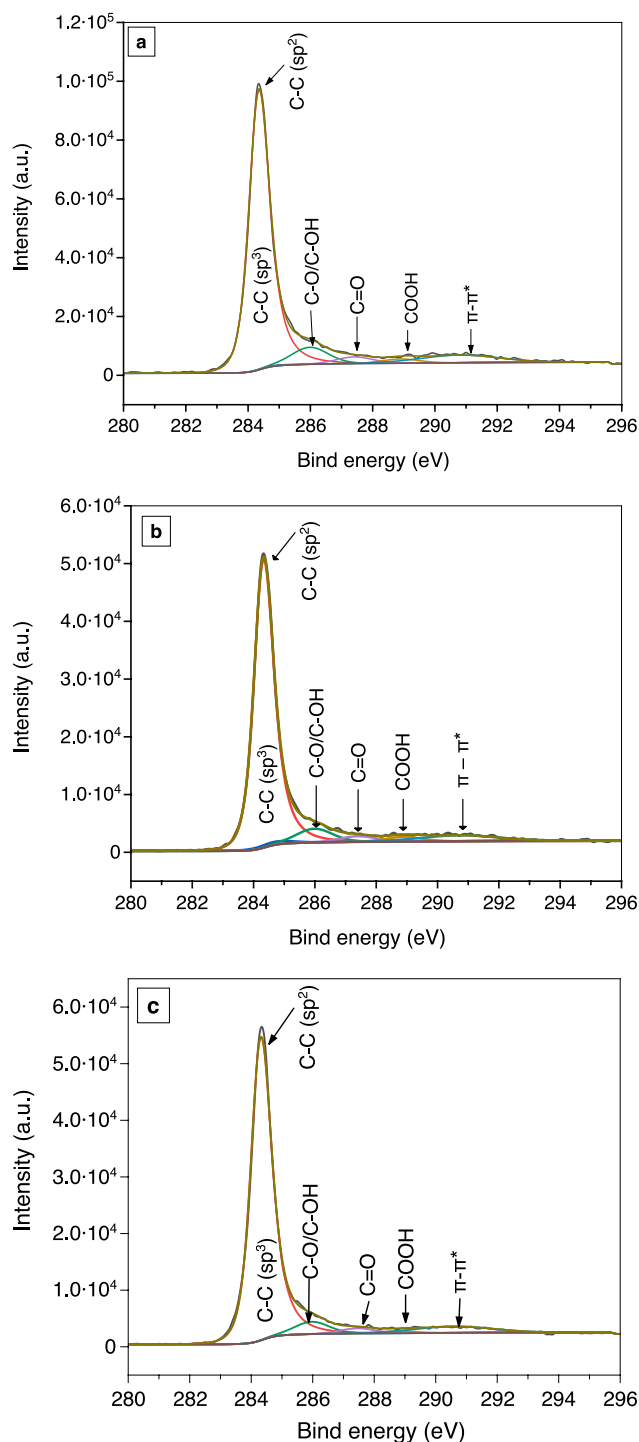


Fig. 7. Detailed C 1s XPS spectra of P-MWCNTs (a), MWCNTs@PDMS-1000(5) (b) and MWCNTs@PDMS-1000(15) (c) nanocomposites.

To analyze the textural characteristics of P-MWCNTs and MWCNTs@PDMS-1000 nanocomposites, low-temperature (77.4 K) nitrogen adsorption–desorption isotherms were recorded using an ASAP 2405 N (Micromeritics Instrument Corp., USA) adsorption analyzer after outgassing the samples at 110 $^{\circ}\text{C}$ for 2 h in a vacuum chamber. The values of the specific surface area (S_{BET}) were calculated according to the standard BET method [34]. The total pore volume V_p was evaluated from nitrogen adsorption at $p/p_0 = 0.98\text{--}0.99$ (p and p_0 denote the equilibrium and saturation pressures of nitrogen at 77.4 K, respectively). The nitrogen desorption data were used to compute the pore size

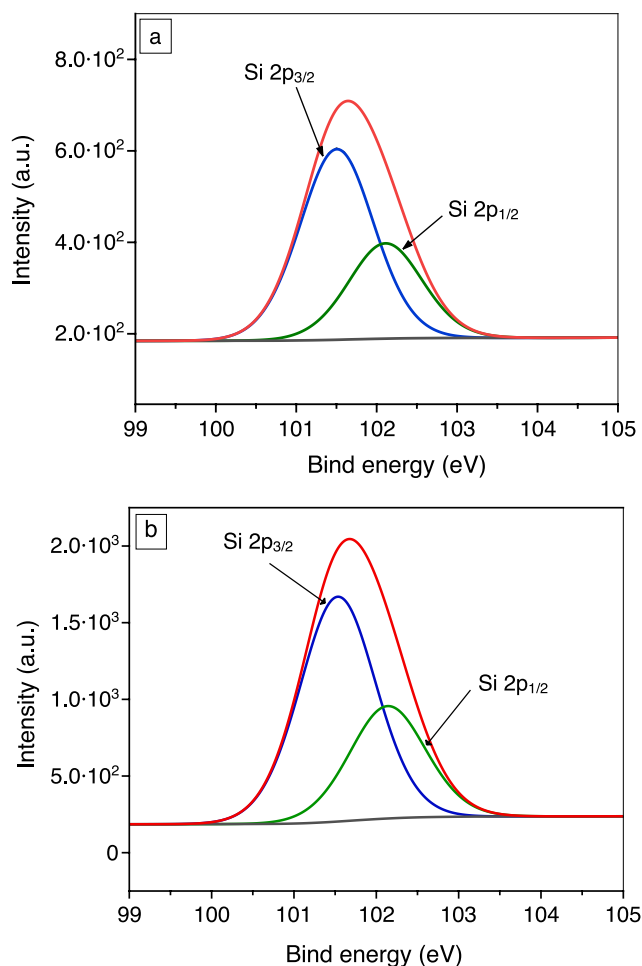


Fig. 8. Detailed Si 2p XPS spectra of MWCNTs@PDMS-1000(5) (a) and MWCNTs@PDMS-1000(15) (b) nanocomposites.

distributions (PSDs, differential $f_V \sim dV_p/dR$ and $f_S \sim dS/dR$) using a self-consistent regularization (SCR) procedure under the non-negativity condition ($f_V \geq 0$ at any R_p) and using a model with slit-shaped, cylindrical pores and voids between nanoparticles (SCV) for MWCNTs@PDMS-1000 nanocomposites and slit-shaped pores for P-MWCNTs [35]. The differential PSDs with respect to the pore volume $f_V \sim dV/dR$, $\int f_V dR \sim V_p$ were re-calculated to the incremental PSD (IPSD) at $\Phi_V(R_i) = (f_V(R_{i+1}) + f_V(R_i))(R_{i+1} - R_i)/2$ at $\sum \Phi_V(R_i) = V_p$. The f_V and f_S functions were also used to calculate contributions of micropores (V_{micro} and S_{micro} at $0.35 \text{ nm} < R < 1 \text{ nm}$), mesopores (V_{meso} and S_{meso} at $1 \text{ nm} < R < 25 \text{ nm}$), and macropores (V_{macro} and S_{macro} at $25 \text{ nm} < R < 100 \text{ nm}$).

Thermo-oxidative stability of the samples was determined using the simultaneous thermal analyzer STA 449 F1 Jupiter (Netzsch, Selb, Germany). The TG, differential TG (DTG) and differential scanning calorimetry (DSC) curves were recorded over the 30–1000 °C range at a heating rate of 10 °C/min in the synthetic air atmosphere (50 mL/min) using a TGA–DSC sensor type S. The samples (mass $\sim 4 \text{ mg}$) were placed in the alumina crucible. The empty Al_2O_3 crucible was used as a reference. Parameters such as ΔH , $\Delta m_{250-500}$ and $\Delta m_{500-720}$ were determined using the NETZSCH Proteus data analysis program (software version 6.1). The gaseous products emitted during the decomposition of materials were analyzed using a quadrupole mass spectrometer QMS 403D Aëolos (Netzsch, Selb, Germany) coupled on-line to the thermal analyzer.

The Digidrop GBX Contact Angle Meter (France) equipped with a video camera and firm software was used in the water contact angle

(WCA, θ) and sliding angle (SA, θ) measurements. To measure the advancing contact angle (ACA), a 6 μL droplet of the water was gently settled on the surface samples and then 2 μL of the liquid was sucked into the microsyringe and the receding contact angle was measured (RCA). The values of WCA were determined using the Win Drop++ program [36]. To obtain the averaged WCA values, the measurements were performed for 10 water droplets put on each sample. The measurements were conducted at 20 °C and the relative humidity RH = 50 %. In order to measure the SA, a 6 μL droplet of the water was placed on the surface, then the entire chamber with the sample was deflected at a speed of 0.3°/s. The whole process was filmed. After the droplet slipped, the filming was finished and the frame on which the droplet began to roll down was selected and the sliding angle corresponding to this frame was read from the device's software.

The apparent surface free energy of the specified surfaces was calculated according to the Neumann equation, which allows estimating the surface free energy of a solid surface by the contact angle of one probe liquid:

$$\gamma_{SL} = \gamma_{LV} + \gamma_{SV} - 2\sqrt{\gamma_{LV}\gamma_{SV}}e^{-\beta(\gamma_{LV}-\gamma_{SV})^2}, \quad (1)$$

which in connection with the Young's equation gives:

$$\cos\theta = -1 + 2\sqrt{\frac{\gamma_{SV}}{\gamma_{LV}}}e^{-\beta(\gamma_{LV}-\gamma_{SV})^2}, \quad (2)$$

where $\beta = 0.000125 \text{ (mJ/m}^2\text{)}^{-2}$ is an experimental value [37].

Electrical measurements were made using a S-1060 probe station (Signatone, Gilroy, USA). A 2410 sourcemeter unit (Keithley, Cleveland, USA) was used for a continuous voltage application. Voltage was increased from 0.01 V to 10 V in a logarithmic sweep in a step-like shape. Current values were measured after a stabilization time of 1.5 s. The current–voltage characteristics (I - V curves) of P-MWCNTs and MWCNTs@PDMS-1000 composites were obtained in air atmosphere. Before the experiment, the powder samples were mechanically pressed in the form of the disc with a diameter of 15 mm and a thickness of approximately 1.5 mm, and then coated with silver paste on both sides followed by curing at 80 °C for 2 h to facilitate the electrical characterization.

3. Results and discussion

3.1. ATR-FTIR

The FTIR spectra of P-MWCNTs, MWCNTs@PDMS-1000 nanocomposites and neat PDMS-1000 are presented in Fig. 2. The P-MWCNTs have no apparent peaks. For neat PDMS-1000 spectrum, all the characteristic bands corresponding to the groups in the polymer structure are present. As can be seen in Fig. 2 (curve 2), PDMS-1000 exhibits absorption bands at 785 cm^{-1} ($\delta(\text{SiO}_2)$), at 1008 and 1096 cm^{-1} (Si–O–Si stretching), at 1261 cm^{-1} (deformation Si–C), and 2968 and 2909 cm^{-1} (asymmetric C–H stretching in Si–CH₃) [38]. The observed doublet bands at 1008 and 1096 cm^{-1} are characteristic of linear PDMS-1000. Accordingly, the same characteristic polymer bands are observed in the synthesized MWCNTs@PDMS-1000 nanocomposites, which indicates an effective surface modification. The bands at 803 cm^{-1} assigned to Si–CH₃, at 1261 cm^{-1} (Si–C deformation in Si–CH₃) and doublet attributed asymmetric stretching vibration of Si–O–Si observed at 1022 and 1096 cm^{-1} confirm the presence of PDMS-1000 adsorbed on the surface of MWCNTs in nanocomposites [39,40].

3.2. XRD

X-ray diffraction is a valuable instrument for elucidating the structure of carbon nanotubes and their polymer nanocomposites [41]. The XRD data for P-MWCNTs and MWCNTs@PDMS-1000 nanocomposites

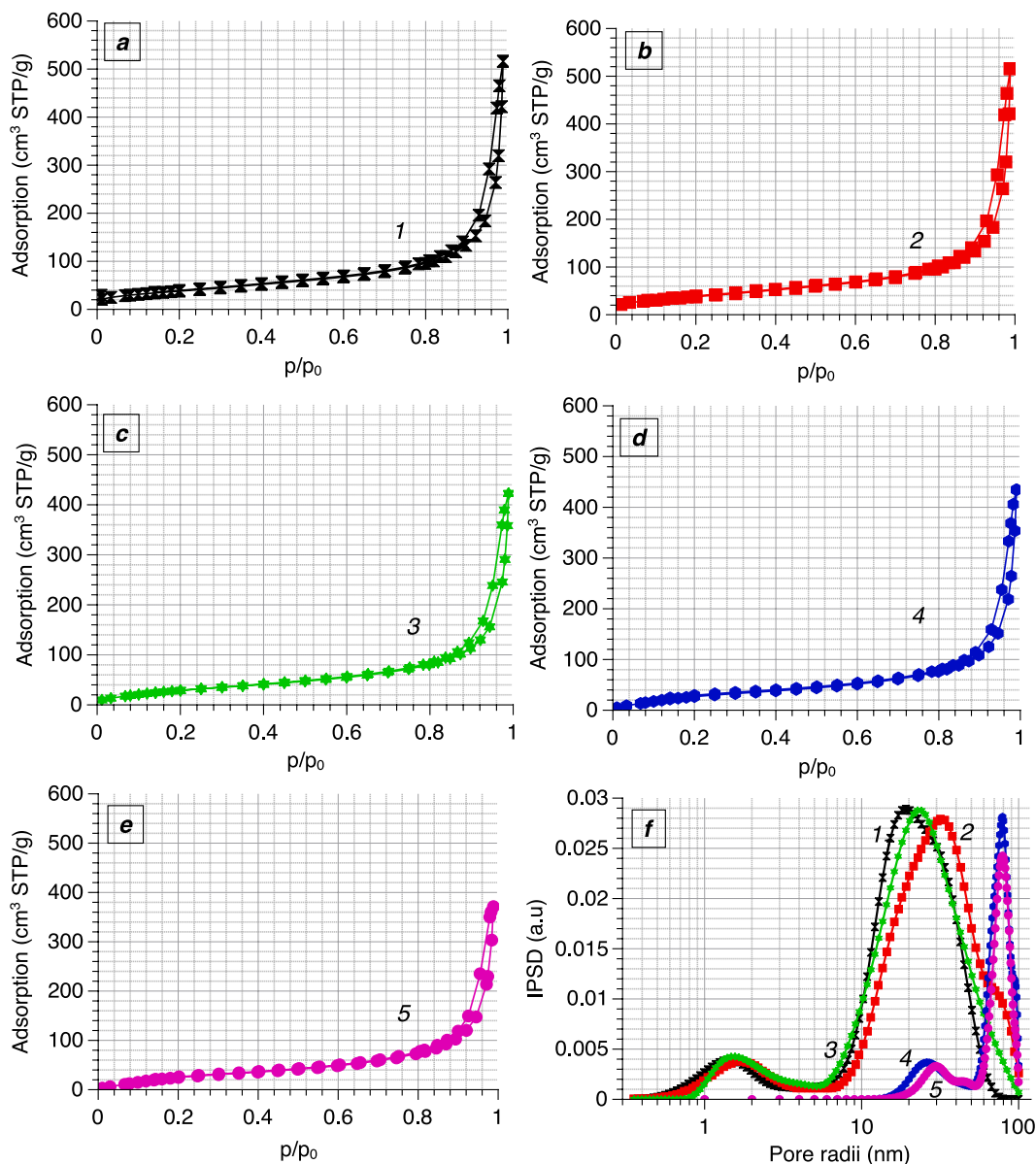


Fig. 9. Nitrogen adsorption–desorption isotherms (a–e) and incremental pore size distributions (f) for P-MWCNTs (curve 1), MWCNTs@PDMS-1000(5) (curve 2), MWCNTs@PDMS-1000(10) (curve 3), MWCNTs@PDMS-1000(15) (curve 4) and MWCNTs@PDMS-1000(20) (curve 5) samples.

are shown in Fig. 3. The characteristic peaks at $2\theta \sim 26^\circ$, $\sim 43^\circ$, $\sim 53^\circ$ and $\sim 78^\circ$ corresponds to (002), (100), (004) and (110) planes of typical graphite, respectively, and matched well for all samples. In addition, the intensity of (002) and (100) peaks for the polymer nanocomposites are reduced compared to P-MWCNTs, indicating the decreases of the crystallinity. Moreover, one can observe a characteristic broad peak located at 12° (Fig. 3, curve 3), which corresponds to the tetragonal unit cell of the PDMS' crystalline phase; this semi-crystalline nature of PDMS has been previously reported in the literature data [42]. Carbon impurities and metal catalyst particles used to produce carbon nanotubes were not identified by XRD method for all samples investigated. Therefore, the XRD patterns were used to calculate the average coherence length or mean crystalline size along the c -axis (L_c) of MWCNTs from the position and full width at half maximum (FWHM) of the (002) peak using the Debye-Scherrer formula [43]. The value of the interlayer spacing $d_{(002)}$ was measured by the Bragg's law [44]. L_c of P-MWCNTs, MWCNTs@PDMS-1000(5) and MWCNTs@PDMS-1000(20) nanocomposites is close to 5 nm. The d_{002} value for all samples derived from this XRD patterns is 0.34 nm (at $2\theta = 26.08^\circ$), which is

slightly higher than that of the perfect graphite ($d_{002} = 0.335$ nm). The very similar values indicate that the crystalline organization remains almost the same after physical absorption of PDMS-1000 on the carbon nanotubes surfaces and correspond to hexagonal crystalline graphite between graphene nanosheets. The mean number of graphitic walls (n) calculated by the Eq. (3) is estimated to be 15 layers:

$$n = L_c/d_{(002)}, \quad (3)$$

where $d_{(002)}$ is the interlayer spacing between the adjacent graphite layers (nm).

3.3. SEM and TEM

The external topography of P-MWCNTs and polymer nanocomposites was revealed by SEM which is presented in Fig. 4. The statistical diameter distribution of with the average values of MWCNTs before and after modification with PDMS-1000 is shown in Fig. 4(b, d, f); the addition of polymer slightly increases slightly the diameters of carbon nanotubes. Fig. 4(a, c, e) show that the P-MWCNTs and

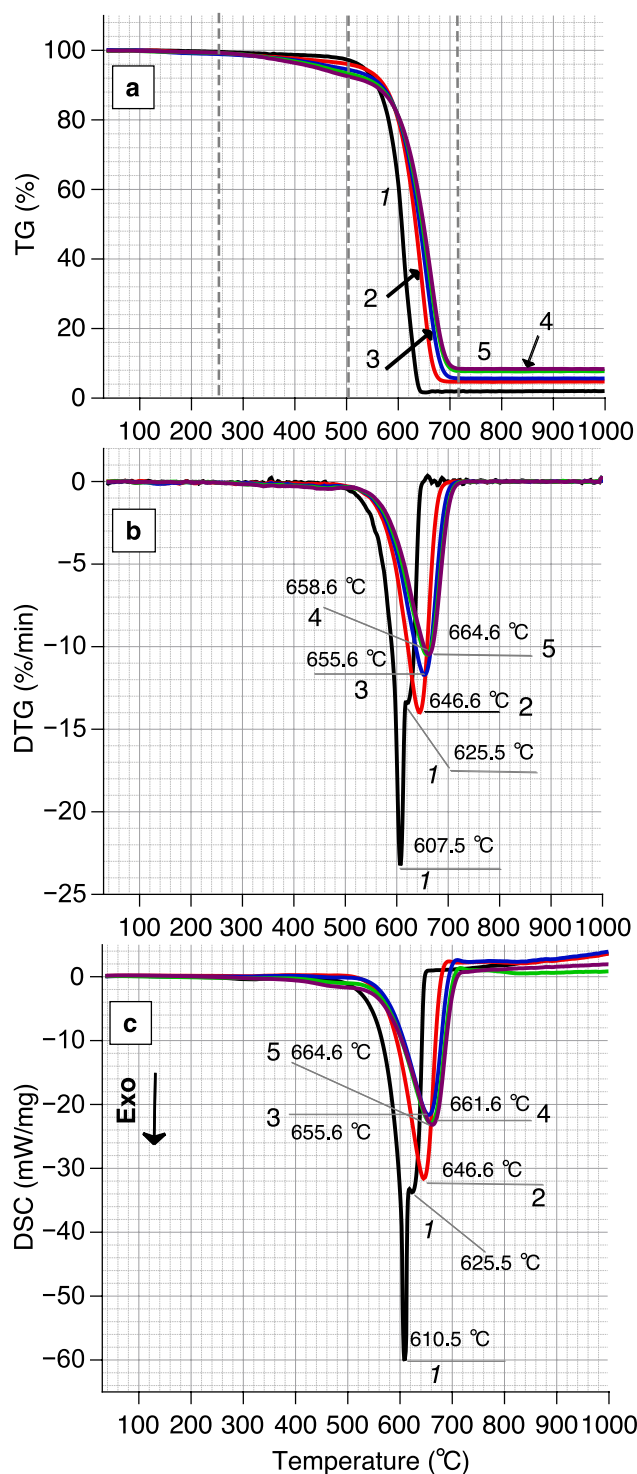


Fig. 10. TG (a), DTG (b) and DSC (c) curves of P-MWCNTs (curve 1), MWCNTs@PDMS-1000(5) (curve 2), MWCNTs@PDMS-1000(10) (curve 3), MWCNTs@PDMS-1000(15) (curve 4) and MWCNTs@PDMS-1000(20) (curve 5) samples.

MWCNTs@PDMS-1000 nanocomposites have a tubular structure on a scale of 1 μm and are bundled together in agglomerates by intermolecular Van der Waals forces.

The morphology of P-MWCNTs and MWCNTs@PDMS-1000 nanocomposites were further characterized by TEM (Fig. 5). Moreover, the inner diameter (Fig. 5b, e, h) and the outer diameter (Fig. 5c, f, i) for these samples are presented. The corresponding TEM images clearly

show the formation of well-developed crystal planes, which are identified as flexible graphite layers and without significant contamination. As can be seen from Fig. 5, the outer diameters of carbon nanotubes are similar for the three examined samples and are close to 15 nm with an average number of layers close to 14–15. The inner diameter is 5–7 nm for P-MWCNTs and MWCNTs@PDMS-1000 nanocomposites, respectively. The average interlayer distance was found to be 0.33 nm in the TEM images. The TEM observations confirm that the polymer adsorption does not damage the graphene layer organization. These findings (i.e., interlayer spacing, average number of graphitic walls) are in full agreement with the data obtained as a result of XRD calculations (paragraph 3.2).

3.4. Raman spectra

Raman spectroscopy can demonstrate even very small alterations in the structures of CNTs, making it a useful tool for the characterization of these materials before and after modification [45]. The Raman spectra of the P-MWCNTs and polymer nanocomposites were measured (Fig. 6). There were observed the following characteristic bands of MWCNTs were observed: D band at $\sim 1315\text{ cm}^{-1}$, G band at $\sim 1610\text{ cm}^{-1}$ and G' band at $\sim 2630\text{ cm}^{-1}$. The D band indicates the presence of disordered amorphous carbon. The G band corresponds to the graphitic nature of the sample that is, crystallinity of the sample, and the G' band arises from the two-phonon, second-order scattering process that results in the creation of an inelastic phonon [46]. It is known that the latter mentioned mode is sensitive to an increase in defect density, but not as significantly as the first-order mode. The intensity of G' band largely depends on the metallicity of the carbon nanotubes [47].

Standard approaches to use of Raman spectroscopy to assess purity are based on the relative intensity ratio of the D band peak and the G band peak (I_D/I_G). Interpretation of I_D/I_G data is complicated due to the effect of carbon impurities on these intensities. DiLeo et al. [48] published a paper showing that the ratio using the G' band peak represents a more accurate alternative for measuring the quality and purity of MWCNTs. In addition, the relative intensities of bands G' and G ($I_{G'}/I_G$) and bands G' and D ($I_{G'}/I_D$), which are considered to be a long-range order indicator and are sensitive to the overall crystalline quality of the graphitic network [49], respectively, have been also evaluated. The relative intensities of the D/G, G'/G, and G'/D ratios are presented in Fig. S1 (Supporting information). The higher the I_D/I_G ratio, the more defects (sp^3 connections) are present relative to what is predicted (sp^2 connections). This ratio for P-MWCNTs is 2.01. After adsorption of 20 wt % polymer, the I_D/I_G ratio slightly increased to 2.13, indicating that after physical adsorption of PDMS-1000 the structure of MWCNTs did not change mainly compared to P-MWCNTs. An insignificant reduction of the G'/G and G'/D ratios of the modified MWCNTs compared to the P-MWCNTs reveals a little larger density of lattice defects after physical adsorption of PDMS-1000 on the carbon nanotubes surfaces.

In addition, the intensity of the G'-peak for the MWCNTs@PDMS-1000(20) sample (Fig. 6, curve 5) is reduced compared to P-MWCNTs (Fig. 6, curve 1) as it becomes less ordered (i.e., more impurities or the addition of the polymer). These results are in good agreement with the data reported in the literature for carbon-nanostructured materials [50,51]. For graphitic materials, the I_D/I_G ratio can be also used to calculate the in-plane crystalline size, L_a , using the following equation [52]: $L_a\text{ (nm)} = 2.4 \times 10^{-10} \times \lambda^4 \times (I_D/I_G)^{-1}$, where λ is the laser excitation wavelength (514 nm in the current study). Based on the data presented in Fig. S1, the in-plane crystalline sizes of P-MWCNTs and MWCNTs@PDMS-1000(20) nanocomposite were calculated to be 8.3, and 7.9 nm respectively. The value of L_a allows to indirectly estimate the density of defects in terms of crystallite size. The in-plane size of graphitic crystallites does not change largely after the physical polymer modification of carbon nanotubes surfaces.

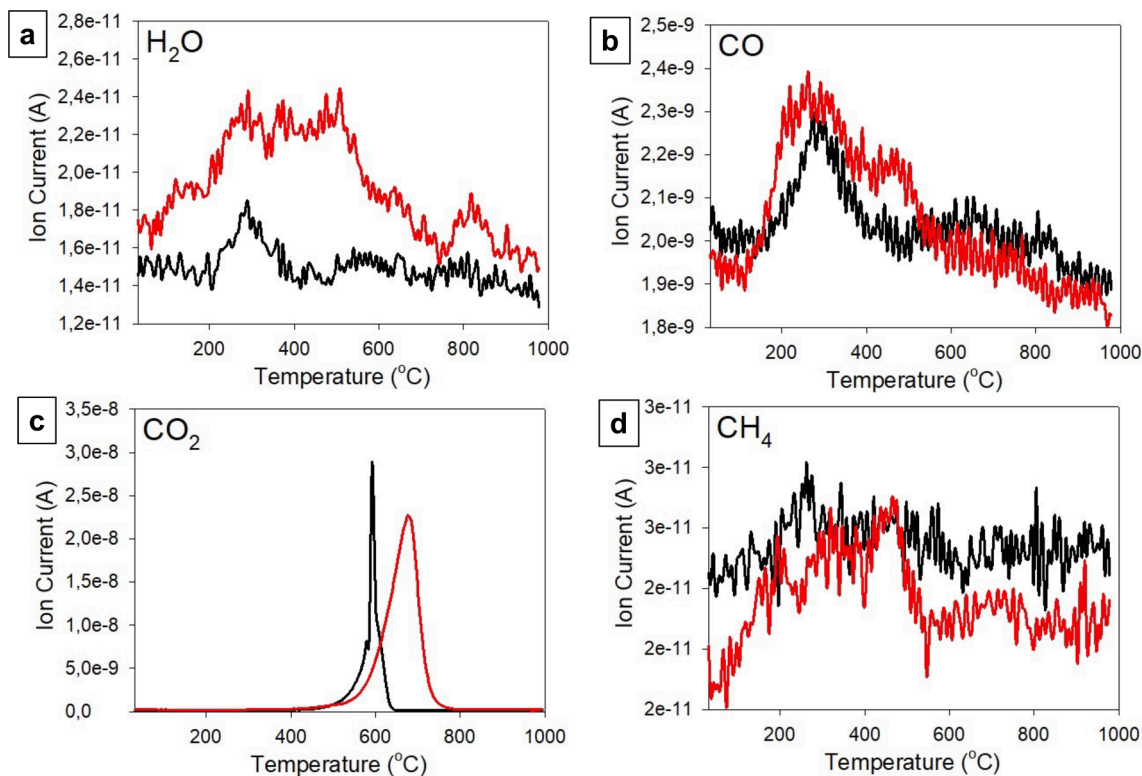


Fig. 11. MS profiles of the main gaseous products of the decomposition for P-MWCNTs (black curves) and MWCNTs@PDMS-1000(15) nanocomposite (red curves): (a) m/z 18 (H_2O); (b) m/z 28 (CO); (c) m/z 44 (CO_2); (d) m/z 16 (CH_4) obtained in the synthetic air atmosphere. (For interpretation of the references to colour in this figure legend, the reader is referred to the web version of this article.)

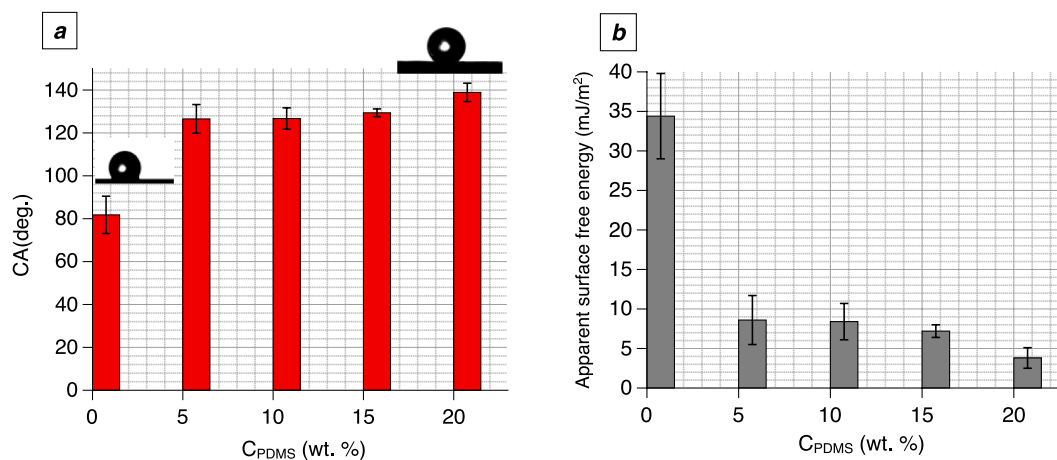


Fig. 12. Dependence of the water contact angle of nanocomposites (a) and the apparent surface free energy (b) on the contents of PDMS-1000 adsorbed onto the MWCNTs surfaces.

3.5. X-ray photoelectron spectroscopy (XPS)

XPS studies were performed on P-MWCNTs, MWCNTs@PDMS-1000 (5) and MWCNTs@PDMS-1000 (15) samples to determine the relative atomic percentages of C, O, and Si in each sample (Table 1) as well as identify changes in the surface chemical composition of carbon nanotubes after physical modification with polymer. The full range of XPS spectra shows the presence of O and C on the surface of all samples (Fig. S2). In addition, we observe an additional typical peak of Si 2p in the XPS spectra of polymer nanocomposites which confirms the successful modification of the carbon nanotubes with PDMS (Table 1, Fig. S2b,c). These results were also confirmed by ATR-FTIR and XRD

data analysis (paragraphs 3.1 and 3.2).

In Fig. 7 shows the XPS C 1s curve-fitted spectra for carbon nanotubes before and after physical adsorption of PDMS. Fitting of C 1s XPS spectra was provided according to the model proposed by Biesinger [53]. For all samples (Fig. 7) C 1s was deconvoluted into six peaks. The peaks located at 284.3 eV and 284.7 eV corresponds to C–C bonds with sp^2 hybridization and C–C bonds with sp^3 hybridization. The next peak observed at 286.0 eV can be associated to the contribution of both C–O and C–OH groups [54]. The last three peaks centered at 287.4 eV, 288.9 eV and 290.8 eV are identified, which corresponds to carbonyl (C=O), carboxyl (–COOH) functionalities and shake-up feature typical of aromatic structures or $\pi - \pi^*$ shake-up, respectively [55]. The C 1s spectra

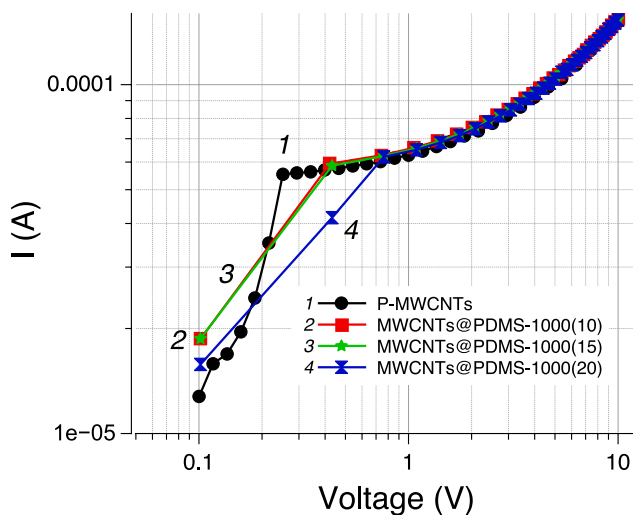


Fig. 13. The current–voltage characteristics of P-MWCNTs (1) and MWCNTs@PDMS-1000 nanocomposites (2–4).

of polymer nanocomposites are similar to the spectra of P-MWCNTs; however, the peak areas for the 284.3 eV peak were increased (Fig. 7c) compared to the peak area of the P-MWCNTs sample. After adsorption of the polymer, a decrease in the peak areas of carbon–oxygen groups (C–O, C=O and –COOH) was observed (Table S1).

We performed additionally deconvolution of the O 1 s band for MWCNTs@PDMS-1000 composites, as shown in Fig. S3. The main component at 531.8 eV can be attributed to the C–O–Si band [56], and the intensity of this peak increases significantly with increasing amount of PDMS onto the MWCNTs surface (Fig. S3). Analysis of the Si 2p spectrum is very informative for evaluating the type of bonds that Si atoms establish. The XPS signal of Si 2p electrons was deconvoluted into two peaks (Fig. 8) observed at 101.5 and 102.1 eV, which can be attributed to the Si–O bonds within PDMS and to the bonding of silicon with three by oxygen atoms, respectively, which compared to those found in the literature [57]. It is important to note that with an increase in the content of PDMS in the nanocomposites, a clear increase in the intensity of Si 2p subpeaks was observed (Fig. 8 and Fig. S2).

3.6. Textural characterization

Nitrogen adsorption–desorption isotherms, pore size distribution profiles and calculated textural parameters of MWCNTs before and after the polymer adsorption are given in Fig. 9 and Table S2, respectively. As shown in Fig. 9a–e, the isotherms are typical for a mesoporous material with a hysteresis loop at high partial pressures. The pore size distribution (Fig. 9f) indicates that the polymer nanocomposites with a small amount of PDMS-1000 (5–10 wt%) exhibit textural behaviour similar to P-MWCNTs. In addition, IPSD curves display clearly the meso/macroporous nature of MWCNTs@PDMS-1000 nanocomposites with the increasing content of the polymer up to 20 wt% (Fig. 9f, curves 4–5). P-MWCNTs are characterized by a larger specific surface area and mesoporous structure compared to the MWCNTs@PDMS-1000 nanocomposites (Table S2). The large macroporosity is due to the packing of nanotubes, which have a large anisotropy, and in this case the pores correspond to the voids between the particles as can be seen on the SEM images (Fig. 4). In the composite materials, the tendency to pack the modified carbon nanotubes similarly to the original MWCNTs remains, and the relative contribution of mesopores decreases slightly with an increase in the content of PDMS-1000. The decrease in porosity for the sample of the composite with the maximum content of polymer (20 wt%) is associated with both a denser packing of the modified carbon nanotubes in the composite and with a slight increase in their diameter after modification (Figs. 4, 5).

3.7. Thermal analysis

The thermo-oxidative stability and degradation processes for the MWCNTs@PDMS-1000 nanocomposites with different amounts of adsorbed polymer were analyzed using the thermogravimetric analysis (TGA) and differential scanning calorimetry. Fig. 10 represents the TG, DTG and DSC traces for all samples under the oxidative conditions. TGA can be used to characterize the purity of a material. The thermal parameters of P-MWCNTs and polymer nanocomposites are also given in Table S3. The T_{\max} is often defined as the thermal stability of the material. The residual mass in the TGA of MWCNTs is usually attributed to the metal catalyst used to manufacture the nanotubes, as well as the oxidation products of the catalyst [58]. The data of thermal analysis coupled with mass spectrometry (MS) allow to determine the release of various gases during the decomposition of functional groups on the surface of P-MWCNTs and polymer composites (Fig. 11).

As shown in Fig. 10a,b, P-MWCNTs are thermally stable up to 500 °C and decomposed completely at 650 °C due to the oxidation of CNTs by oxygen, which corresponds well to the literature data [59]. Two partially-overlapping peaks with maxima at 607.5 °C and 625.5 °C on the DTG/DSC curves for P-MWCNTs can be attributed to the burning temperature of amorphous and crystalline carbon, respectively [46]. The oxidation rate of carbon nanotubes is lower than that of amorphous carbon due to the layered configuration of graphene sheets. According to the TG and DSC curves (Fig. 10a,c), the thermo-oxidative destruction of MWCNTs@PDMS-1000 nanocomposites occurs in two stages in the range of 250–500 and 500–720 °C. All TG/DTG/DSC curves (Fig. 10) of polymer nanocomposites show a common behaviour, thus the used amount of MWCNTs in the composites does not result in essential difference in the decomposition process of the polymer. The thermal decomposition of adsorbed PDMS molecules on the carbon nanotubes surfaces in the first stage at temperatures between 250 and 500 °C in an oxygen-containing atmosphere is mainly related to depolymerization of the siloxane chains and rupture of the polymer backbone with the formation of cyclic siloxane oligomers [60,61]. In this temperature range, small emissions of gaseous products such as water, CO, and hydrocarbons were observed (Fig. 11a,b,d). At the second stage (500–720 °C), all polymer nanocomposites show a sharp weight loss, which corresponds to the oxidation of CH₃ groups of polymer to SiO₂, water and CO₂ (Fig. 11a,c) as well as carbon of graphene structures in agreement with the literature data [61]. In general, these processes are accompanied by an exothermic effect, which is confirmed by the DSC curves for the studied samples (Fig. 10c). As can be seen from the data in Table S3, mass losses ($\Delta m_{250-500}$) increases proportionally to the amount of adsorbed polymer. There is no weight loss above 720 °C (Fig. 10a). The residues content of the nanocomposites was found to be higher (about 8.5 wt% in the case of MWCNTs@PDMS-1000(20) sample) than that of the P-MWCNTs (2.0 wt%). As follows from Table S3, the char residue of the composite increased with the increasing the polymer amount. The remaining part of the residue was probably due to the SiO₂ phase because of the oxidation of PDMS in the air condition [62]. These changes are reflected in the photographs of the residues in the crucible after the thermal analysis of the studied samples (Fig. S4).

The Fig. 10b illustrates that the temperatures at which polymer nanocomposites begin to decompose are higher than that of P-MWCNTs. It can be clearly noticed that the addition of the polymer enhanced the thermo-oxidative stability of the nanocomposites up to 664.6 °C in the case of the MWCNTs@PDMS-1000(20) sample, which is 57 °C higher compared to P-MWCNTs. This finding can be explained by the cross-linking of the polymer onto the carbon nanotubes surfaces, which leads to the loss of free mobility of the chains, while the density of the PDMS layer increases, and therefore the final destruction occurs at a higher temperature.

3.8. Hydrophobicity

The water contact angle was measured to evaluate the hydrophobic surface characteristics of P-MWCNTs and MWCNTs@PDMS-1000 nanocomposites. The WCA was estimated depending on the polymer concentration in the samples, and the results are given in Fig. 12a. The WCA on the P-MWCNTs surface had a value of $81.8^\circ \pm 8.7^\circ$. The contact angle of water droplets on neat PDMS was 107° as reported in the literature [63]. The addition of 5 wt% of PDMS-1000 gave a WCA value of the MWCNTs@PDMS-1000(5) nanocomposite of $126.5^\circ \pm 6.7^\circ$, which was significantly increased compared to P-MWCNTs and neat PDMS. The water contact angle value of the composite was much higher when the wt. % polymer content increased to 20 wt% at $138.9^\circ \pm 4.3^\circ$. This could be due to the synergistic impact of the MWCNTs surface roughness and the hydrophobic polymer. For the surface of MWCNTs@PDMS-1000(20) nanocomposite the sliding angle is 38° and recording can be found in the Supporting Video. The calculated surface free energies are significantly higher for the P-MWCNTs than for the MWCNTs@PDMS-1000 nanocomposites (Fig. 12b). The specific surface area of polymer nanocomposites decreases with the increasing PDMS-1000 content (Table S2). It was found that the calculated the apparent surface free energy decreased extremely from $34.4 \pm 5.4 \text{ mJ/m}^2$ to $3.8 \pm 1.3 \text{ mJ/m}^2$ for the MWCNTs@PDMS-1000 composites with the increasing amount of PDMS-1000. Larger changes in the interactions of composites with water occur evidently before the PDMS monolayer formation as the interactions of MWCNTs surface (hydrophilic) and PDMS (hydrophobic) with water differ strongly.

3.9. Electrical behaviour

The effect of polymer concentration on *I-V* characteristic of MWCNTs is illustrated in Fig. 13. It was observed that as the applied potential difference rises, the associated electric current values increase for all the studied samples. It can be seen that *I-V* characteristics have a non-linear behaviour, independent of the polymer content. The absence of difference on the *I-V* characteristic between P-MWCNTs and PDMS-1000 modified might be the result of a single percolation electrical path that is created during the pressing of the pellets. On the other hand, the same response for all measured samples indicates unchanged electrical transport of the carbon nanotubes, even after the PDMS-1000 surface modification. The non-linear behaviour of MWCNTs has been already been observed by other authors [64].

4. Conclusions

In this experimental study, hydrophobic MWCNTs@PDMS-1000 nanocomposites with different polymer contents were effectively prepared by the one-stage synthesis. The nanomaterials were characterized in terms of structure and surface morphology, hydrophobicity, thermo-oxidative stability, and electrical behaviour. The ATR-FTIR investigation revealed the presence of characteristic bands of the polymer structure (asymmetric C–H stretching in Si–CH₃) for neat PDMS-1000 and for nanocomposites, indicating successful modification of the MWCNTs surface. The Raman results provided slight changes in the I_D/I_G , I_G/I_G and I_G/I_D ratios for modified MWCNTs compared to P-MWCNTs. The XRD patterns of polymer nanocomposites are similar to P-MWCNTs. According to the SEM evaluation, the outer diameters of MWCNTs before and after modification are similar for the studied samples, and are equal to 18 and 20 nm, respectively. From XRD/Raman patterns and SEM/TEM analysis, it can be concluded that modified MWCNTs is still had the same cylinder wall structure and interplanar spacing as before (0.34 nm). Thus, the structure of MWCNTs is protected even after the physical adsorption of polymer. However, the nitrogen adsorption–desorption analysis shows a change in the textural characteristics of the nanocomposites compared to the P-MWCNTs: both the specific surface area and the pore volume decrease due to PDMS-1000

adsorption.

Furthermore, the water contact angle measurement and apparent surface free energy reduction to $3.8 \pm 1.3 \text{ mJ/m}^2$ in the case of the largest amount of polymer (20 wt%) demonstrated that those the MWCNTs@PDMS-1000 nanocomposites surfaces are much more hydrophobic than of P-MWCNTs. One of the main conclusions of this work is that the addition of polymer improves the thermo-oxidative stability of the obtained polymer nanocomposites by increasing the temperature of maximum thermal degradation rate (T_{max}) up to 664.6°C in the case of the MWCNTs@PDMS-1000(20) nanocomposite, as shown by the results obtained from the TGA/DTG/DSC experiments. In addition, TGA-MS analysis revealed that CO₂ was the main gaseous product during the thermo-oxidative degradation of PDMS on MWCNT surfaces in the higher temperature region. The electrical properties of P-MWCNTs and MWCNTs@PDMS-1000 nanocomposites were investigated as the function of polymer content and applied voltage. The lack of difference in the *I-V* characteristics between P-MWCNTs and after polymer modification can be explained by a single percolation electrical path created during pellets pressing in the case of these measurements.

The studied nanocomposites with enhanced hydrophobicity and higher thermo-oxidative stability can be incorporated into a silicon-based matrix as a new strategy to tailor the dispersion and chemical compatibility of hierarchical MWCNTs@PDMS@Polymer materials to address electrical, thermal or mechanical properties for various application in nanoelectronic devices, e.g. to manage the electrical field in insulation systems [65]. Further research on the inclusion of such nanocomposites into a silicone-based polymer is underway [66].

CRedit authorship contribution statement

Iryna Sulym: Writing – original draft, Validation, Methodology, Investigation, Formal analysis, Data curation, Conceptualization. **Olena Goncharuk:** Writing – review & editing, Investigation, Formal analysis, Data curation. **Liudmyla Storozhuk:** Writing – review & editing, Formal analysis. **Konrad Terpiłowski:** Writing – review & editing, Resources, Formal analysis, Data curation. **Dariusz Sternik:** Resources, Investigation. **Eugen Pakhlov:** Investigation. **Sombel Diahham:** Writing – review & editing. **Zarel Valdez-Nava:** Writing – review & editing, Resources, Investigation.

Declaration of competing interest

The authors declare that they have no known competing financial interests or personal relationships that could have appeared to influence the work reported in this paper.

Data availability

Data will be made available on request.

Acknowledgments

The authors gratefully appreciate the financial support from the International Visegrad Fund (Dr. I. Sulym, Contract number 52210724; D. Sc. O. Goncharuk, Contract number 52211441; Dr.hab. K. Terpiłowski, Contract numbers 52211441 and 52210724). I.S. acknowledges PAUSE Program from the College de France and PAUSE – ANR Ukraine program (Ukrainian scientists support, ANR-19-CE09-0007-03) for the financing support. The authors would like to express their gratitude to Dr. Y.I. Sementsov (Chuiko Institute of Surface Chemistry, NASU, Kyiv, Ukraine) for providing the initial carbon nanotubes as well as to Prof. V. M. Gun'ko for the developing and providing the program for the pore size distribution calculation.

Appendix A. Supplementary data

Supplementary data to this article can be found online at <https://doi.org/10.1016/j.apsusc.2024.160405>.

References

- [1] K. Sheng, X. Dong, Z. Chen, Z. Zhou, Y. Gu, J. Huang, Increasing the surface hydrophobicity of silicone rubber by electron beam irradiation in the presence of a glycerol layer, *Appl. Surf. Sci.* 591 (2022) 153097, <https://doi.org/10.1016/j.apsusc.2022.153097>.
- [2] G. Zheng, D. Zhang, C. Zheng, Y. Yao, Z. Long, Facile fabrication of biomimetic superoleophobic composite coating via Schiff base reaction and self-assembly, *Prog. Org. Coat.* 142 (2020) 105568, <https://doi.org/10.1016/j.porgcoat.2020.105568>.
- [3] T. Maitra, M.K. Tiwari, C. Antonini, P. Schoch, S. Jung, P. Eberle, D. Poulikakos, On the nanoengineering of superhydrophobic and impalement resistant surface textures below the freezing temperature, *Nano Lett.* 14 (2014) 172–182, <https://doi.org/10.1021/nl4037092>.
- [4] E. Celia, T. Darmanin, E.T. de Givenchy, S. Amigoni, F. Guittard, Recent advances in designing superhydrophobic surfaces, *J. Colloid Interface Sci.* 402 (2013) 1–18, <https://doi.org/10.1016/j.jcis.2013.03.041>.
- [5] R. Ghamarpoo, M. Jamshidi, Preparation of Superhydrophobic/Superoleophilic nitrile rubber (NBR) nanocomposites contained silanized nano silica for efficient oil/water separation, *Sep. Purif. Technol.* 291 (2022) 120854, <https://doi.org/10.1016/j.seppur.2022.120854>.
- [6] G. Zheng, Y. Cui, Z. Jiang, M. Zhou, Y. Yu, P. Wang, Q. Wang, Superhydrophobic, photothermal, and UV-resistant coatings obtained by polydimethylsiloxane treating self-healing hydrophobic chitosan-tannic acid surface for oil/water separation, *J. Chem. Eng.* 473 (2023) 145258, <https://doi.org/10.1016/j.cej.2023.145258>.
- [7] L. Gong, W. Yang, Y. Sun, C. Zhou, F. Wu, H. Zeng, Fabricating tunable superhydrophobic surfaces enabled by surface-initiated emulsion polymerization in water, *Adv. Funct. Mater.* 33 (2023) 2214947, <https://doi.org/10.1002/adfm.202214947>.
- [8] E. Ozkan, M. Garren, J. Manuel, M. Douglass, R. Devine, A. Mondal, A. Kumar, M. Ashcraft, R. Pandey, H. Handa, Superhydrophobic and conductive foams with antifouling and oil-water separation properties, *ACS Appl. Mater. Interfaces.* 15 (2023) 7610–7626, <https://doi.org/10.1021/acsami.2c22180>.
- [9] Y.A. Mehanna, E. Sadler, R.L. Upton, A.G. Kempchinsky, Y. Lu, C.R. Crick, The challenges, achievements and applications of submersible superhydrophobic materials, *Chem. Soc. Rev.* 50 (2021) 6569–6612, <https://doi.org/10.1039/D0CS01056A>.
- [10] A. Ribeiro, B. Soares, J. Furtado, A. Silva, N. Couto, Superhydrophobic nanocomposite coatings based on different polysiloxane matrices designed for electrical insulators, *Prog. Org. Coat.* 168 (2022) 106867, <https://doi.org/10.1016/j.porgcoat.2022.106867>.
- [11] H.-E.-D. Saleh, S.M.M. El-Sheikh, *Perspective of Carbon Nanotubes, BoD-Books on Demand, InTech (2019)*.
- [12] Z. Spital'sky, D. Tasis, K. Papagelis, C. Galiotis, Carbon nanotube-polymer composites: chemistry, processing, mechanical and electrical properties, *Prog. Polym. Sci.* 35 (2010) 357–401, <https://doi.org/10.1016/j.progpolymsci.2009.09.003>.
- [13] R. Chakradhar, G. Prasad, P. Bera, C. Anandan, Stable superhydrophobic coatings using PVDF-MWCNT nanocomposite, *Appl. Surf. Sci.* 301 (2014) 208–215, <https://doi.org/10.1016/j.apsusc.2014.02.044>.
- [14] R.H. Baughman, A.A. Zakhidov, W.A. De Heer, Carbon nanotubes—the route toward applications, *J. Sci.* 297 (2002) 787–792, <https://doi.org/10.1126/science.1060928>.
- [15] U. Szeluga, S. Pusz, B. Kumanek, K. Olszowska, A. Kobylukh, B. Trzebiecka, Effect of graphene filler structure on electrical, thermal, mechanical, and fire retardant properties of epoxy-graphene nanocomposites—a review, *Crit. Rev. Solid State Mater. Sci.* 46 (2021) 152–187, <https://doi.org/10.1080/10408436.2019.1708702>.
- [16] S. Malekie, F. Ziaie, A two-dimensional simulation to predict the electrical behavior of carbon nanotube/polymer composites, *J. Polym. Eng.* 37 (2017) 205–210, <https://doi.org/10.1515/polyeng-2015-0511>.
- [17] M. Terrones, Science and technology of the twenty-first century: synthesis, properties, and applications of carbon nanotubes, *Annu. Rev. Mater. Res.* 33 (2003) 419–501, <https://doi.org/10.1146/annurev.matsci.33.012802.100255>.
- [18] J. Yan, Y.G. Jeong, Multiwalled carbon nanotube/polydimethylsiloxane composite films as high performance flexible electric heating elements, *Appl. Phys. Lett.* 105 (2014) 51907, <https://doi.org/10.1063/1.4892545>.
- [19] J. Gu, P. Xiao, J. Chen, J. Zhang, Y. Huang, T. Chen, Janus polymer/carbon nanotube hybrid membranes for oil/water separation, *ACS Appl. Mater. Interfaces.* 6 (2014) 16204–16209, <https://doi.org/10.1021/am504326m>.
- [20] H.M. Alghamdi, A. Rajeh, Synthesis of CoFe₂O₄/MWCNTs nanohybrid and its effect on the optical, thermal, and conductivity of PVA/CMC composite as an application in electrochemical devices, *J. Inorg. Organomet. Polym. Mater.* 32 (2022) 1935–1949, <https://doi.org/10.1007/s10904-022-02322-z>.
- [21] N. Roy, A.K. Bhowmick, In situ preparation, morphology and electrical properties of carbon nanofiber/polydimethylsiloxane nanocomposites, *J. Mater. Sci.* 47 (2012) 272, <https://doi.org/10.1007/s10853-011-5795-y>.
- [22] P.K. Sharma, N. Gupta, P.I. Dankov, Analysis of dielectric properties of polydimethylsiloxane (PDMS) as a flexible substrate for sensors and antenna applications, *IEEE Sens. J.* 21 (2021) 19492–19504, <https://doi.org/10.1109/JSEN.2021.3089827>.
- [23] A.A. Yetisgin, H. Sakar, H. Bermek, L. Trabzon, Production of elastomer-based highly conductive hybrid nanocomposites and treatment with sulfuric acid, *J. Polym. Eng.* 41 (2021) 467–479, <https://doi.org/10.1515/polyeng-2021-0040>.
- [24] R. Ariati, F. Sales, A. Souza, R.A. Lima, J. Ribeiro, Polydimethylsiloxane composites characterization and its applications: A review, *Polymers* 13 (2021) 4258, <https://doi.org/10.3390/polym13234258>.
- [25] A. Beigbeder, M. Linares, M. Devalckenaere, P. Degée, M. Claes, D. Beljonne, R. Lazzaroni, P. Dubois, CH- π interactions as the driving force for silicone-based nanocomposites with exceptional properties, *Adv. Mater.* 20 (2008) 1003–1007, <https://doi.org/10.1002/adma.200701497>.
- [26] M. Norkhairunnisa, A. Azizan, M. Mariatti, H. Ismail, L. Sim, Thermal stability and electrical behavior of polydimethylsiloxane nanocomposites with carbon nanotubes and carbon black fillers, *J. Compos. Mater.* 46 (2012) 903–910, <https://doi.org/10.1177/0021998311412985>.
- [27] R. Han, Y. Li, Q. Zhu, K. Niu, Research on the preparation and thermal stability of silicone rubber composites: A review, *JCOMC* 8 (2022) 100249, <https://doi.org/10.1016/j.jcomc.2022.100249>.
- [28] I. Sulym, A. Kubiak, K. Jankowska, D. Sternik, K. Terpilowski, Y. Sementsov, M. Borysenko, A. Derylo-Marczewska, T. Jesionowski, Superhydrophobic MWCNTs/PDMS-nanocomposite materials: Preparation and characterization, *Physicochem. Probl. Miner. Process.* 55 (2019) 1394–1400, <https://doi.org/10.5277/ppmp19057>.
- [29] I. Sulym, J. Zdarta, F. Ciesielczyk, D. Sternik, A. Derylo-Marczewska, T. Jesionowski, Pristine and poly (Dimethylsiloxane) modified multi-walled carbon nanotubes as supports for lipase immobilization, *Mater.* 14 (2021) 2874, <https://doi.org/10.3390/ma14112874>.
- [30] I. Sulym, A. Cetinkaya, M. Yence, M.E. Çorman, L. Uzun, S.A. Ozkan, Novel electrochemical sensor based on molecularly imprinted polymer combined with L-His-MWCNTs@ PDMS-5 nanocomposite for selective and sensitive assay of tetracycline, *Electrochim. Acta.* 430 (2022) 141102, <https://doi.org/10.1016/j.electacta.2022.141102>.
- [31] M. Kartel, Y. Sementsov, S. Mahno, V. Trachevskiy, W. Bo, Polymer composites filled with multiwall carbon nanotubes, *Univ. J. Mater. Sci.* 4 (2016) 23–31, <https://doi.org/DOI:10.13189/ujms.2016.040202>.
- [32] V. Yanchenko, S. Yu, A. Melezhyk, Method of obtaining of catalysts for CVD of carbon nanotubes, *Ukrainian Pat. Application* 20041008154, *Int. Cl. 7 (2004) C01B11*.
- [33] I. Sulym, O. Goncharuk, D. Sternik, K. Terpilowski, A. Derylo-Marczewska, M. V. Borysenko, V.M. Gun'ko, Nanoxide/polymer composites with silica@PDMS and ceria-zirconia-Silica@PDMS: textural, morphological, and hydrophilic/hydrophobic features, *Nanoscale Res. Lett.* 12 (2017) 152, <https://doi.org/10.1186/s11671-017-1935-x>.
- [34] S.J. Gregg, K.S.W. Sing, *Adsorption, Surface Area and Porosity*, Academic Press, London, 1982.
- [35] V.M. Gun'ko, S.V. Mikhailovsky, Evaluation of slitlike porosity of carbon adsorbents, *Carbon* 42 (2004) 843–849, <https://doi.org/10.1016/j.carbon.2004.01.059>.
- [36] E. Chibowski, K. Terpilowski, Surface free energy of sulfur—Revisited: I. Yellow and orange samples solidified against glass surface, *J. Colloid Interface Sci.* 319 (2008) 505–513, <https://doi.org/10.1016/j.jcis.2007.10.059>.
- [37] E. Chibowski, On some relations between advancing, receding and Young's contact angles, *Adv. Colloid Interface Sci.* 133 (2007) 51–59, <https://doi.org/10.1016/j.cis.2007.03.002>.
- [38] J. Raczkowska, S. Prauzner-Bechcicki, J. Lukes, J. Sepitka, A. Bernasik, K. Awsiuk, C. Paluszkievicz, J. Pabijan, M. Lekka, A. Budkowski, Physico-chemical properties of PDMS surfaces suitable as substrates for cell cultures, *Appl. Surf. Sci.* 389 (2016) 247–254, <https://doi.org/10.1016/j.apsusc.2016.07.009>.
- [39] J. Lee, J. Kim, H. Kim, Y.M. Bae, K.H. Lee, H.J. Cho, Effect of thermal treatment on the chemical resistance of polydimethylsiloxane for microfluidic devices, *J. Micromech. Microeng.* 23 (2013) 035007, <https://doi.org/10.1088/0960-1317/23/3/035007>.
- [40] D. Cai, A. Neyer, R. Kuckuk, H.M. Heise, Raman, mid-infrared, near-infrared and ultraviolet-visible spectroscopy of PDMS silicone rubber for characterization of polymer optical waveguide materials, *J. Mol. Struct.* 976 (2010) 274–281, <https://doi.org/10.1016/j.molstruc.2010.03.054>.
- [41] B. Emmanuel, S. Thomas, G. Raghuvaran, D. Sherwood, Simulated XRD profiles of carbon nanotubes (CNTs): An efficient algorithm and a recurrence relation for characterising CNTs, *J. Alloys Compd.* 479 (2009) 484–488, <https://doi.org/10.1016/j.jallcom.2008.12.109>.
- [42] H.D. Shetty, A. Patra, V. Prasad, Polydimethylsiloxane-multiwalled carbon nanotube composite as a metamaterial, *Mater. Lett.* 210 (2018) 309–313, <https://doi.org/10.1016/j.matlet.2017.09.051>.
- [43] B.D. Cullity, S.R. Stock, *Elements of X-ray Diffraction*, 3rd edition, Prentice-Hall, New York, 2001.
- [44] Y. Sheng, X. Tang, E. Peng, J. Xue, Graphene oxide based fluorescent nanocomposites for cellular imaging, *J. Mater. Chem. B.* 1 (2013) 512–521, <https://doi.org/10.1039/C2TB00123C>.
- [45] M. Dresselhaus, G. Dresselhaus, A. Jorio, Raman spectroscopy of carbon nanotubes in 1997 and 2007, *J. Phys. Chem. C.* 111 (2007) 17887–17893, <https://doi.org/10.1021/jp071378n>.

- [46] J.H. Lehman, M. Terrones, E. Mansfield, K.E. Hurst, V. Meunier, Evaluating the characteristics of multiwall carbon nanotubes, *Carbon*. 49 (2011) 2581–2602, <https://doi.org/10.1016/j.carbon.2011.03.028>.
- [47] K.K. Kim, J.S. Park, S.J. Kim, H.Z. Geng, K.H. An, C.M. Yang, K. Sato, R. Saito, Y. H. Lee, Dependence of Raman spectra G' band intensity on metallicity of single-wall carbon nanotubes, *Phys. Rev. B*. 76 (2007) 205426, <https://doi.org/10.1103/PhysRevB.76.205426>.
- [48] R.A. DiLeo, B.J. Landi, R.P. Raffaele, Purity assessment of multiwalled carbon nanotubes by Raman spectroscopy, *J. Appl. Phys.* 101 (2007) 064307, <https://doi.org/10.1063/1.2712152>.
- [49] S. Santangelo, G. Messina, G. Faggio, M. Lanza, C. Milone, Evaluation of crystalline perfection degree of multi-walled carbon nanotubes: correlations between thermal kinetic analysis and micro-Raman spectroscopy, *J. Raman Spectrosc.* 42 (2011) 593–602, <https://doi.org/10.1002/jrs.2766>.
- [50] M.A. Hosseini, H. Zare, S. Malekie, Raman spectroscopy of electron irradiated Multi-Walled Carbon Nanotube for dosimetry purposes, *Radiat. Phys. Chem.* 202 (2023) 110535, <https://doi.org/10.1016/j.radphyschem.2022.110535>.
- [51] D. Ryoo, J.Y. Kim, P.K. Duy, S.H. Cho, H. Chung, T.H. Yoon, Fast and non-destructive Raman spectroscopic determination of multi-walled carbon nanotube (MWCNT) contents in MWCNT/polydimethylsiloxane composites, *Analyst*. 143 (2018) 4347–4353, <https://doi.org/10.1039/C8AN00351C>.
- [52] B. Gebhardt, F. Hof, C. Backes, M. Müller, T. Plocke, J. Maultzsch, C. Thomsen, F. Hauke, A. Hirsch, Selective polycarboxylation of semiconducting single-walled carbon nanotubes by reductive sidewall functionalization, *J. Am. Chem. Soc.* 133 (2011) 19459–19473, <https://doi.org/10.1021/ja206818n>.
- [53] M.C. Biesinger, Accessing the robustness of adventitious carbon for charge referencing (correction) purposes in XPS analysis: Insights from a multi-user facility data review, *Appl. Surf. Sci.* 597 (2022) 15368, <https://doi.org/10.1016/j.apsusc.2022.153681>.
- [54] T.I.T. Okpalugo, P. Papakonstantinou, H. Murphy, J. McLaughlin, N.M.D. Brown, High resolution XPS characterization of chemical functionalised MWCNTs and SWCNTs, *Carbon* 43 (2005) 153–161, <https://doi.org/10.1016/j.carbon.2004.08.033>.
- [55] J.V. Rojas, M. Toro-Gonzalez, M.C. Molina-Higgins, C.E. Castano, Facile radiolytic synthesis of ruthenium nanoparticles on graphene oxide and carbon nanotubes, *Mater. Sci. Eng. B*. 205 (2016) 28–35, <https://doi.org/10.1016/j.mseb.2015.12.005>.
- [56] M. Nour, K. Berean, S. Balendhran, J.Z. Ou, J.D. Plessis, C. McSweeney, M. Bhaskaran, S. Sriram, K. Kalantar-zadeh, CNT/PDMS composite membranes for H₂ and CH₄ gas separation, *Int. J. Hydrog. Energy* 38 (2013) 10494–10501, <https://doi.org/10.1016/j.ijhydene.2013.05.162>.
- [57] M. Morra, E. Occhiello, R. Marola, F. Garbassi, P. Humphrey, D. Johnson, On the aging of oxygen plasma-treated polydimethylsiloxane surfaces, *J. Colloid Interface Sci.* 137 (1990) 11–24, [https://doi.org/10.1016/0021-9797\(90\)90038-P](https://doi.org/10.1016/0021-9797(90)90038-P).
- [58] G. Messina, V. Modafferi, S. Santangelo, P. Tripodi, M.G. Donato, M. Lanza, S. Galvagno, C. Milone, E. Piperopoulos, A. Pistone, Large-scale production of high-quality multi-walled carbon nanotubes: Role of precursor gas and of Fe-catalyst support, *Diam. Relat. Mater.* 17 (2008) 1482–1488, <https://doi.org/10.1016/j.diamond.2008.01.060>.
- [59] M.F. Ran, W.J. Sun, Y. Liu, W. Chu, C.F. Jiang, Functionalization of multi-walled carbon nanotubes using water-assisted chemical vapor deposition, *J. Solid State Chem.* 197 (2013) 517–522, <https://doi.org/10.1016/j.jssc.2012.08.014>.
- [60] V.M. Gun'ko, E.M. Pakhlov, O.V. Goncharuk, L.S. Andriyko, Yu.M. Nychiporuk, D. Yu. Balakin, D. Sternik, A. Derylo-Marczewska, Nanosilica modified by polydimethylsiloxane depolymerized and chemically bound to nanoparticles or physically bound to unmodified or modified surfaces: Structure and interfacial phenomena, *J. Colloid Interface Sci.* 529 (2018) 273–282, <https://doi.org/10.1016/j.jcis.2018.06.019>.
- [61] G. Camino, S.M. Lomakin, M. Laguard, Thermal polydimethylsiloxane degradation. Part 2. The degradation mechanisms, *Polymer* 43 (2002) 2011–2015, [https://doi.org/10.1016/S0032-3861\(01\)00785-6](https://doi.org/10.1016/S0032-3861(01)00785-6).
- [62] K. Li, X. Zeng, H. Li, X. Lai, H. Xie, Effects of calcination temperature on the microstructure and wetting behavior of superhydrophobic polydimethylsiloxane/silica coating, *Colloids Surf. A: Physicochem. Eng. Asp.* 445 (2014) 111–118, <https://doi.org/10.1016/j.colsurfa.2014.01.024>.
- [63] B. Ruben, M. Elisa, L. Leandro, M. Victor, G. Gloria, S. Marina, S. Mian K, R. Pandiyan, L. Nadhira, Oxygen plasma treatments of polydimethylsiloxane surfaces: effect of the atomic oxygen on capillary flow in the microchannels, *Nanomicro Lett.* 12 (2017) 754–757, <https://doi.org/10.1049/mnl.2017.0230>.
- [64] K. Kaneto, M. Tsuruta, G. Sakai, W. Cho, Y. Ando, Electrical conductivities of multi-wall carbon nano tubes, *Synth. Met.* 103 (1999) 2543–2546, [https://doi.org/10.1016/S0379-6779\(98\)00221-5](https://doi.org/10.1016/S0379-6779(98)00221-5).
- [65] A. Can-Ortiz, L. Laudebat, Z. Valdez-Nava, S. Diaham, Nonlinear Electrical Conduction in Polymer Composites for Field Grading in High-Voltage Applications: A Review, *Polymers* 13 (2021) 1370, <https://doi.org/10.3390/polym13091370>.
- [66] K. Terpilowski, I. Sulym, O. Goncharuk, E. Pakhlov, Z. Valdez-Nava, Effect of MWCNTs amount on the polymer nanocomposites surface properties, In abstracts, ACC2023, Thessaloniki, Greece, p. 253.